

Instructions to Authors for the Preparation of Papers for the 18th Australian International Aerospace Congress

Please select category below:

Normal Paper

Student Paper

Young Engineer Paper

Consider Probability Hypothesis Density Filtering for Multiple Space Objects Tracking

Yang Yang ^{1,2}, Steve Gehly ³, Han Cai ^{1,2} and Robert Norman ^{1,2}

¹ SPACE Research Centre, School of Science, RMIT University, 124 La Trobe St, Melbourne Victoria, 3000, Australia

² Space Environment Research Centre Limited, Canberra, Australian Capital Territory, 3001, 2610, Australia

³ Space Research Group, UNSW Canberra

Abstract

Space object tracking and surveillance has become an imperative task as the near-Earth space environment has been contaminated and crowded by these objects and their number is still increasing fast due to new launches and break-up/collision events. However, the imperfect orbit dynamics makes this task very challenging. In order to improve the tracking performance for multiple space objects, this paper proposes a consider probability hypothesis density (PHD) filter. In comparison with the conventional PHD filter, this new filter additionally considers an uncertain parameter (i.e., the area-to-mass ratio (AMR)) involved in the orbit dynamics model that leads to inaccurate orbit prediction, and deteriorated tracking and state estimation performances for these objects subsequently. More specifically, the covariance associated with such parameters has been considered via the formulation of Gaussian mixture consider unscented Kalman filtering, based on which the consider PHD filter is implemented. Numerical simulation results indicate the consider PHD filter is more advantageous than a traditional PHD filter that estimates the uncertain model parameters together with other state variables.

Keywords: space tracking, probability hypothesis density filter, consider parameter, area-to-mass ratio

Introduction

Space technology has been beneficial to human beings in many areas since the space era began in the 1950s. Many daily-life services rely on satellites that are orbiting the Earth. However, as the population of residential space objects (RSOs) increases, the near-Earth space becomes congested. It has been reported by the National Aeronautics and Space Administration (America's space agency) that there are more than 5,000,000 pieces of space debris in the near-Earth orbit and this number is still increasing fast, through collisions and further launching of satellites. Among them, over 20,000 space objects have size larger than 10 centimetres [1]. Most of these objects are nonoperational and uncontrolled, and flying at great speeds, hence pose severe threats to operational satellites. In order to avoid collisions between any space objects, the acquisition of accurate and reliable state information of these

threatening objects is necessary, which is the fundamental task that multiple object tracking (MOT) has to solve.

The main objectives of MOT are to detect space objects, maintain their identities, and predict their individual trajectories given applicable observations (e.g., angles, ranges, etc). Classical MOT approaches, e.g., multiple hypotheses tracking (MHT) [2] and joint probabilistic data association (JPDA) [3], generally simplify the MOT problem as multiple single-object tracking problems by way of data associations. A relatively new approach to MOT leverages the theory of random finite sets (RFSs) to represent multi-object states. Unlike MHT and JPDA, RFS filtering realises Bayes' recursion for multi-object densities through time, and no extra data association process is needed [4]. Although the Bayesian multi-object filter is theoretically optimal, it is intractable for most practical applications. Hence, many approximations have been proposed to circumvent the intractability, which can be categorised into two groups, the moment approximation filters and the multi-Bernoulli approximation filters. The former group predict and update only the low-order moment of the multi-object density instead of the full distribution, e.g., the first-order moment, resulting in the probability hypothesis density (PHD) filter [5] and cardinalized PHD filter [6]. The second group approximate the multi-object density by the multi-Bernoulli function, resulting in multi-Bernoulli filters [4] and δ -generalized labeled multi-Bernoulli filters [7].

A prominent challenge arising in space object tracking is uncertainty in the equations of motion resulting from perturbing forces. For example, uncertainties associated with the physical parameters of such an object lead to more difficulties in state estimation. In addition, less accurate state estimation results in uncertain environmental effects on the object, causing poor parameter identification and vice versa.

In order to improve the tracking performance for single and multiple space objects, McCabe and DeMars derived a Gaussian mixture (GM) consider PHD filter based on the linear Bayesian formulations [8]. This work develops the consider scheme in the framework of GM unscented Kalman filtering and applies it to the space tracking problem. In comparison with the conventional PHD filter, this new filter additionally considers an extra uncertain parameter, i.e., the area-to-mass ratio (AMR) involved in the orbit dynamics models that leads to inaccurate orbit prediction, and deteriorated tracking and state estimation performances for these objects subsequently. More specifically, the covariance associated with such a parameter has been considered via the formulation of Gaussian mixture consider unscented Kalman filtering, based on which the consider PHD filter is implemented.

The rest of the paper is organised as follows: Section 2 revisits the Bayesian multi-object filtering theory in a concise way, followed by the general formulation of the PHD filter given in Section 3. Section 4 revisits the consider Kalman filter and Section 5 introduces the Gaussian mixture implementation for PHD recursion and the consider Kalman filter scheme is used in the measurement update step to consider the parametric uncertainty. Three numerical tests for the space tracking application, a simple one and two more realistic ones, have been used to demonstrate the efficacy of the consider PHD filter. The results indicate the consider PHD filter can achieve better state estimation accuracy than a traditional PHD filter that estimates the uncertain model parameters together with other state variables. Finally, some concluding remarks are given.

Bayesian Multi-Object Filtering

In the formulation of RFSs, the system equations for a multi-object system can be expressed as

$$\mathbf{X}_k = \left\{ \mathbf{x}_{k,1}, \dots, \mathbf{x}_{k,N(k)} \right\}, \quad (1)$$

$$Z_k = \{z_{k,1}, \dots, z_{k,M(k)}\}. \quad (2)$$

At the time epoch k , there are $N(k)$ objects $x_{k,1}, \dots, x_{k,N(k)}$, respectively taking values from an unlabelled state space \mathbb{X} , and $M(k)$ measurements $z_{k,1}, \dots, z_{k,M(k)}$, respectively taking values from an observation space \mathbb{Z} .

Chapman-Kolmogorov Equation

Suppose that the multi-object density is denoted as $\pi(X|Z)$ at the current time epoch, then the Chapman-Kolmogorov equation is used to propagate it to the next time epoch:

$$\pi_{k|k-1}(X_k | Z_{1:k-1}) = \int f_{k|k-1}(X_k | X) \pi_{k-1}(X | Z_{1:k-1}) \delta X, \quad (3)$$

where X_k denotes the superposition of surviving, spawn and new born objects, and the integral is a set integral defined for any multi-object transition kernel function $f: \mathcal{F}(\mathbb{X}) \rightarrow \mathbb{R}$ by:

$$\int f(X) \delta X = \sum_{i=0}^{\infty} \frac{1}{i!} \int f(\{x_1, \dots, x_i\}) d(x_1, \dots, x_i). \quad (4)$$

Bayesian Inference

Given the measurement history $Z_{1:k}$ up to the time epoch k , the multi-object posterior density π_k can be calculated via the Bayesian inference:

$$\pi_k(X|Z) = \frac{g_k(Z_k | X_k) \pi_{k|k-1}(X_k | Z_{1:k-1})}{\int g_k(Z_k | X) \pi_{k|k-1}(X | Z_{1:k-1}) \delta X}, \quad (5)$$

where g_k denotes the multi-object likelihood function and the multiple-target measurement Z_k is given by [5]:

$$Z_k = C_k \cup \left[\bigcup_{x \in X_k} \psi_k(x) \right]. \quad (6)$$

The measurement model in Eq.(6) considers detection uncertainty and false alarm (clutter measurement). A given object $x_k \in X_k$ is either detected with probability p_D or missed with probability $1-p_D$. If detected, the probability density of receiving an observation $z_k \in \mathbb{Z}$ from x_k is $g_k(z_k | x_k)$. Then an RFS ψ_k is used to express the detection uncertainty, i.e., it takes on z_k if detected or \emptyset if missed. The clutter measurement C_k is problem independent, which is elaborated in the subsection of Clutter Model.

Eqs (3) and (5) are required to be calculated recursively in the filtering process. However, they are generally computationally intractable for practical applications. Many approximation approaches have been proposed to obtain tractable solutions for Bayesian multi-object filtering, one of which is the PHD filter.

Probability Hypothesis Density Filter

Instead of propagating the entire multi-object posterior probability density, the PHD filter propagates only the first order moment, or intensity. The PHD recursion is given as below [5]:

$$v_{k|k-1}(x_A) = \int p_{S,k}(\xi) f_{k|k-1}(x_A | \xi) v_{k-1}(\xi) d\xi + \int \beta_{k|k-1}(x_A | \xi) v_{k-1}(\xi) d\xi + v_{B,k}(x_A), \quad (7)$$

$$v_k(x_A) = [1 - p_{D,k}(x_A)]v_{k|k-1}(x_A) + \sum_{z \in \mathbb{Z}_k} \frac{p_{D,k}(x_A)g_k(z|x_A)v_{k|k-1}(x_A)}{\kappa_k(z) + \int p_{D,k}(\xi)g_k(z|\xi)v_{k|k-1}(\xi)d\xi}, \quad (8)$$

where v_k and $v_{k|k-1}$ indicate the intensities associated with the multi-object posterior density π_k and the multi-object predicted density $\pi_{k|k-1}$; $p_{S,k}(\xi)$ is the surviving probability of an object that exists at time k given that its previous state is ξ ; $\beta_{k|k-1}(\cdot|\xi)$ is the intensity of the RFS $B_{k|k-1}$ spawned by an object with previous state ξ ; $v_{B,k}(\cdot)$ is the intensity of the birth PHD Γ_k ; $p_{D,k}(x)$ is the probability of detection given a state x ; $\kappa_k(\cdot)$ is the intensity of clutter PHD C_k .

Via Eqns. (7)-(8), PHD filters reduce the integration to the single-object state space \mathbb{X} instead of the multi-object state space $\mathcal{F}(\mathbb{X})$. They provide multi-object state estimates and the total number of objects; however, they do not retain object identity information. Panta et al proposed a relatively simple and effective modification of the PHD recursion to identify the object with a separate track table [9]. The object identity is ignored in this work. The total mass $\hat{N} = \int v(x)dx$ gives the expected number of objects. To further simplify the integrals in Eqns. (7)-(8), Vo et al. proposed a Gaussian mixture to approximate the PHD [5], this leads to the formulation of GM PHD introduced in the next section.

Birth Model

In the space tracking mission, when a new-birth object without prior information is coming into the sensor, an initial orbit determination (IOD) process is needed. Classical IOD solutions require several measurements to determine a six-dimensional orbit. Instead, birth models using the constrained admissible region (CAR) and the probabilistic admissible region (PAR) [10, 11] have been developed for space object tracking. Recently authors also proposed a BVP (boundary value problem) approach and applied it to the labeled multi-Bernoulli filter [12]. This study only uses CAR for IOD of new objects.

Clutter Model

For space tracking applications, the clutter is modelled as a Poisson RFS C_k with the intensity uniformly distributed in the field of view (FOV) of the sensor (e.g., telescope camera) [13]:

$$\kappa(z) = \lambda_c \cdot \mathcal{U}(z), \quad (9)$$

$$\mathcal{U}(z) = \begin{cases} 1/V_s, & \text{if } z \in \text{FOV}; \\ 0, & \text{if } z \notin \text{FOV}, \end{cases} \quad (10)$$

where λ_c is the mean return rate of the measurement clutter, and V_s is the sensor volume.

Consider Unscented Kalman Filtering

Given the systematic equations for a single object in Eqns. (1)-(2):

$$\begin{aligned} x_{A,k} &= f(x_{A,k-1}) + w_k, & w_k &\sim \mathcal{N}(x_A; 0, Q_k) \\ z_k &= g(x_{A,k}) + v_k, & v_k &\sim \mathcal{N}(z; 0, R_k) \end{aligned} \quad (11)$$

where $x_A = (x, c)^T$ consists of both state variables and parameters, and the subscript k indicates the time index. Additive process noise w and measurement noise v are considered. Specifically, these distributions are assumed to be Gaussian. Frequently, state estimation of the system in Eqn (11) depends on parameters whose values are only known imprecisely. In

some cases, these uncertain parameters can be estimated together with state variables. Unfortunately, these parameters may not all be observable, so the resulting estimates may be deteriorated to some extent. For these reasons, Schmidt proposed an approach to account for the uncertainties associated with these nuisance parameters by including the propagation and update of their covariance into the conventional Kaman filter, which is the basic concept of the so-called Schmidt-Kalman filter or consider Kalman filter (CKF). The CKF is derived by first applying the Kalman filter scheme to the augmented system x_A [14]. The consider unscented Kalman filter (CUKF) algorithm is summarized as below. Different from Ref. [15], a formulation of unscaled CUKF used in [16] is given here.

Time Update

$$P_{k-1}^+ = S_{k-1} S_{k-1}^T, \quad (12)$$

$$S_{k-1} = \begin{bmatrix} s_{1,k-1} & \cdots & s_{n,k-1} \end{bmatrix}, \quad (13)$$

$$\mathcal{X}_{l,k-1} = \begin{cases} x_{A,k-1}^+ + \sqrt{n} s_{l,k-1}, & l = 1, \dots, n; \\ x_{A,k-1}^+ - \sqrt{n} s_{l-n,k-1}, & l = n+1, \dots, 2n; \end{cases} \quad (14)$$

$$\mathcal{X}_{l,k} = f(\mathcal{X}_{l,k-1}) \quad \forall l \in \{1, \dots, 2n\}, \quad (15)$$

$$m_{k/k-1} = \sum_{l=1}^{2n} \frac{1}{2n} \mathcal{X}_{l,k}, \quad (16)$$

$$P_{k/k-1}^- = \sum_{l=1}^{2n} \frac{1}{2n} (\mathcal{X}_{l,k} - m_{k/k-1})(\mathcal{X}_{l,k} - m_{k/k-1})^T + Q_{k-1}.$$

Measurement Update

$$\mathcal{Z}_{l,k} = g(\mathcal{X}_{l,k}) \quad \forall l \in \{1, \dots, 2n\}, \quad (17)$$

$$m(z) = \sum_{l=1}^{2n} \frac{1}{2n} \mathcal{Z}_{l,k}, \quad (18)$$

$$P_{zz,k} = \sum_{l=1}^{2n} \frac{1}{2n} (\mathcal{Z}_{l,k} - m(z))(\mathcal{Z}_{l,k} - m(z))^T + R_k,$$

$$P_{xz,k} = \sum_{l=1}^{2n} \frac{1}{2n} (\mathcal{X}_{l,k} - m_{k/k-1})(\mathcal{Z}_{l,k} - m(z))^T, \quad (19)$$

$$K_k = P_{xz,k} (P_{zz,k})^{-1} = \begin{bmatrix} K_{x,k} \\ K_{c,k} \end{bmatrix},$$

$$K_k = P_{xz,k} (P_{zz,k})^{-1} = \begin{bmatrix} K_{x,k} \\ 0 \end{bmatrix},$$

$$m_{x,k|k} = m_{x,k|k-1} + K_{x,k} (z_k - m(z)), \quad (20)$$

$$m_{c,k|k} = m_{c,k|k-1},$$

$$P_{x,k|k} = P_{x,k|k-1} - K_{x,k} P_{zz,k} K_{x,k}^T, \quad (21)$$

$$P_{xc,k|k} = P_{xc,k|k-1} - K_{x,k} P_{zz,k} K_{c,k}^T = P_{cx,k|k}^T,$$

$$P_{c,k|k} = P_{c,k|k-1}. \quad (22)$$

The Gaussian Mixture PHD Recursion

The posterior intensity $v_{k-1}(x)$ at time $k-1$ and its prediction to time k are both given as forms of Gaussian mixture:

$$v_{k|k-1}(x_A) = \sum_{i=1}^{J_{k|k-1}} \omega_{k|k-1}^{(i)} p_{\mathcal{N}}(x_A; m_{k|k-1}^{(i)}, P_{k|k-1}^{(i)}), \quad (23)$$

$$v_{k-1}(x_A) = \sum_{i=1}^{J_{k-1}} \omega_{k-1}^{(i)} p_{\mathcal{N}}(x_A; m_{k-1}^{(i)}, P_{k-1}^{(i)}), \quad (24)$$

where

$$p_{\mathcal{N}}(x_A; m, P) = [\det(2\pi P)]^{-1/2} \exp\left[-\frac{1}{2}(x_A - m)^\top P^{-1}(x_A - m)\right], \quad (25)$$

with

$$m = \begin{bmatrix} x \\ c \end{bmatrix}, \quad P = \begin{bmatrix} P_x & P_{xc} \\ P_{cx} & P_c \end{bmatrix}, \quad (26)$$

and J_{k-1} and $J_{k|k-1}$ are numbers of Gaussian mixture components. x_A is an augmented vector, in which x denotes the orbital state vector and c indicates the consider orbital parameter vector. It is assumed hereafter that the probability of detection is state-independent, and the clutter intensity is uniform distributed over the tracking region, i.e.,

$$p_{D,k}(x) \equiv p_{D,k}, \quad \kappa_k^{(i)} \equiv \kappa_k.$$

Time update

Without considering the object spawning, the predicted intensity for time k is also a Gaussian mixture given by:

$$v_{k|k-1}(x_A) = v_{S,k|k-1}(x_A) + v_{B,k}(x_A), \quad (27)$$

$$v_{B,k}(x_A) = \sum_{i=1}^{J_{B,k}} \omega_{B,k}^{(i)} p_{\mathcal{N}}(x_A; m_{B,k}^{(i)}, P_{B,k}^{(i)}), \quad (28)$$

$$v_{S,k|k-1}(x) = p_{S,k} \sum_{i=1}^{J_{k-1}} \omega_{k-1}^{(i)} p_{\mathcal{N}}(x_A; m_{S,k|k-1}^{(i)}, P_{S,k|k-1}^{(i)}), \quad (29)$$

$$m_{S,k|k-1}^{(i)} = \sum_{j=0}^{2n} \omega_{\mathcal{X}}(j) f(\mathcal{X}_{k-1}^{(i)}(j)), \quad (30)$$

$$P_{S,k|k-1}^{(i)} = \sum_{j=0}^{2n} w_p(j) (f(\mathcal{X}_{k-1}^{(i)}(j)) - m_{S,k|k-1}^{(i)}) (f(\mathcal{X}_{k-1}^{(i)}(j)) - m_{S,k|k-1}^{(i)})^\top + Q_{k-1}. \quad (31)$$

Measurement Update

Substituting the predicted PHD in Eqn 12 into the second item of the numerator of Eqn 8 yields:

$$\begin{aligned} & p_{D,k} \sum_{i=1}^{J_{k|k-1}} \omega_{k|k-1}^{(i)} p_{\mathcal{N}}(z; h(x_A), R) p_{\mathcal{N}}(x_A; m_{k|k-1}^{(i)}, P_{k|k-1}^{(i)}) \\ &= p_{D,k} \sum_{i=1}^{J_{k|k-1}} \omega_{k|k-1}^{(i)} p_{\mathcal{N}}(z; z^{(i)}, P_{zz}^{(i)}) p_{\mathcal{N}}(x_A; m_{k|k}^{(i)}(z), P_{k|k}^{(i)}). \end{aligned} \quad (32)$$

Similarly, the denominator of Eqn 8 can be written as:

$$\kappa_k(z) + p_{D,k} \sum_{i=1}^{J_{k|k-1}} \omega_{k|k-1}^{(i)} p_{\mathcal{N}}(z; z^{(i)}, P_{zz}^{(i)}). \quad (33)$$

The posterior intensity at time k is a Gaussian mixture given by:

$$v_k(x_A) = [1 - p_{D,k}(x_A)] v_{k|k-1}(x_A) + \sum_{z \in Z_k} v_{D,k}(x_A, z), \quad (34)$$

where

$$\begin{aligned} v_{D,k}(x_A, z) &= \sum_{i=1}^{J_{k|k-1}} \omega_k^{(i)}(z) p_{\mathcal{N}}(x_A; m_{k|k}^{(i)}(z), P_{k|k}^{(i)}), \\ \omega_k^{(i)}(z) &= \frac{p_{D,k} \omega_{k|k-1}^{(i)} q_k^{(i)}(z)}{\kappa_k + p_{D,k} \sum_{\ell} \omega_{k|k-1}^{(\ell)} q_k^{(\ell)}(z)}, \\ q_k^{(i)}(z) &= p_{\mathcal{N}}(z; z_k^{(i)}, P_{zz,k}^{(i)}). \end{aligned} \quad (35)$$

$z_k^{(i)}, P_{zz,k}^{(i)}$ are calculated using sigma points $\mathcal{X}_k^{(i)}(j)$:

$$\begin{aligned} z_k^{(i)} &= \sum_{j=0}^{2n} \omega_{\mathcal{X}}(j) h(\mathcal{X}_k^{(i)}(j)), \\ P_{zz,k}^{(i)} &= \sum_{j=0}^{2n} w_p(j) (h(\mathcal{X}_k^{(i)}(j)) - z_k^{(i)}) (h(\mathcal{X}_k^{(i)}(j)) - z_k^{(i)})^{\top} + R_k, \\ P_{xz,k}^{(i)} &= \sum_{j=0}^{2n} w_p(j) (\mathcal{X}_k^{(i)}(j) - m_{S,k|k-1}^{(i)}) (h(\mathcal{X}_k^{(i)}(j)) - z_k^{(i)})^{\top}, \\ K_k^{(i)} &= P_{xz,k}^{(i)} (P_{zz,k}^{(i)})^{-1} = \begin{bmatrix} K_{x,k}^{(i)} \\ K_{c,k}^{(i)} \end{bmatrix} = \begin{bmatrix} K_{x,k}^{(i)} \\ 0 \end{bmatrix}, \\ m_{x,k|k}^{(i)} &= m_{x,k|k-1}^{(i)} + K_{x,k}^{(i)} (z - z_k^{(i)}), \\ m_{c,k|k}^{(i)} &= m_{c,k|k-1}^{(i)}, \\ P_{x,k|k}^{(i)} &= P_{x,k|k-1}^{(i)} - K_{x,k}^{(i)} P_{zz,k}^{(i)} (K_{x,k}^{(i)})^{\top}, \\ P_{xc,k|k}^{(i)} &= P_{xc,k|k-1}^{(i)} - K_{x,k}^{(i)} P_{zz,k}^{(i)}, \\ K_{c,k}^{\top} &= (P_{cx,k|k}^{(i)})^{\top} P_{c,k|k}^{(i)} = P_{c,k|k-1}^{(i)}, \\ P_{k|k}^{(i)} &= \begin{bmatrix} P_{x,k|k}^{(i)} & P_{xc,k|k}^{(i)} \\ P_{cx,k|k}^{(i)} & P_{c,k|k}^{(i)} \end{bmatrix}. \end{aligned} \quad (36)$$

Multi-Object State Extraction

The object states are extracted with weights larger than a given threshold (e.g., 0.5 [5]):

$$\hat{N}_k = \{N_k^i : \omega_k^i > 0.5\}. \quad (37)$$

The multi-object state is given by:

$$X_{k|k} = \{x_{k|k}^i : N_k^i \in \hat{N}_k, j = 1, \dots, k\}. \quad (38)$$

Numerical Simulations

To compare the consider PHD filter and PHD filter in the MOT application, two numerical examples are tested in this paper: a simple scenario of two space objects and two more realistic scenarios of tracking threeobjects. In the first scenario, no miss-detected, spawn, birth and death objects are considered. The measurement is free of clutter. Two space objects (Object 1 and 2) are tracked from the beginning to the end. The second scenario considers all the above models except target spawning. One more target (Object 3) is considered as a birth from the 5th epoch and one target (Object 2) disappears from the 21th epoch. Similar with the second scenario, the third one considers three space objects (Object 1, 4, 5) in the MOT scenario, with the third one as birth. All the objects are generated by adding noise of [100m, 1e-6, 1e-6 rad, 1e-6 rad, 1e-6 rad, 1e-6 rad] (standard deviation) to the first set of Keplerian elements in order to test the filters for closely located space objects. The initial Keplerian elements are given in Table 1. Initial state and parameter values for filters are randomly generated with standard deviations given in Table 2. A single ground station is used for simulating the optical observations with the Earth centred Earth fixed (ECEF) coordinates given in Table 3. Force models and parameters for space objects are summarised in Table 4. Table 5 gives the process noise added for the position, velocity and the parameter of AMR. AMR is accounted for in addition to orbital state in the consider PHD filter. Standard deviations for angular and angular-rate measurements are given in Table 6. To compare the PHD filters, a consistent metric, i.e., optimal sub-pattern assignment (OSPA), is used for performance evaluation [17]. All OSPA calculations in this paper are parameterised by a p -norm of 2, cutoff values of 50 km for position and 10 m/s for velocity respectively.

Table 1: GEO objects initial Keplerian elements ^[18]

Object	a (km)	e	i (rad)	Ω (rad)	ω (rad)	M (rad)
1	42164.573	2.878e-4	0.006	278.657	139.8697	91.432
2	41169.822	2.1e-4	1.303	189.101	9.869	-51.024
3	42164.283	2.878e-4	-0.003	4.863	2.441	1.754
4	42164.628	2.871e-4	1.047e-4	4.863	2.441	1.596
5	42164.576	2.882e-4	1.047e-4	4.863	2.441	1.596

Table 2: Initial state standard deviations

Position	Velocity	AMR
$\sigma_x = \sigma_y = \sigma_z = 1$ km	$\sigma_{v_x} = \sigma_{v_y} = \sigma_{v_z} = 1$ m/s	0.2

Table 3: Ground station ECEF coordinate (Socorro, NM, US)

Position (km)	Velocity (m/s)
-1519.509, -5077.663, 3550.820	0, 0, 0

Table 4: GEO objects force models and parameters

Parameters	Truth	Filter
Mass		100 kg
Satellite model		Cannon-ball
Earth gravity field		GGM03S
Gravity degree/order	6×6	4×4
Third-body gravity		Sun and Moon
Solar radiation pressure		Considered
A/m value	0.5	Additional 20% random uniform value
Coordinates transformations	IERS1996/IAU1980 transformations ¹⁶	
Integrator	Variable order variable step-size multistep method	

Table 5: Process noise standard deviations

Position	Velocity	AMR
$\sigma_x = \sigma_y = \sigma_z = 10 \text{ m}$	$\sigma_{v_x} = \sigma_{v_y} = \sigma_{v_z} = 0.01 \text{ m/s}$	0.1

Table 6: Measurement standard deviations

	Angles	Angular Rates
Test 1	$\sigma_\alpha = \sigma_\delta = 0.4 \text{ arcsec}$	$\sigma_{\dot{\alpha}} = \sigma_{\dot{\delta}} = 0.07 \text{ arcsec/s}$
Test 2	$\sigma_\alpha = \sigma_\delta = 2 \text{ arcsec}$	$\sigma_{\dot{\alpha}} = \sigma_{\dot{\delta}} = 0.35 \text{ arcsec/s}$
Test 3	$\sigma_\alpha = \sigma_\delta = 3 \text{ arcsec}$	$\sigma_{\dot{\alpha}} = \sigma_{\dot{\delta}} = 0.35 \text{ arcsec/s}$

Table 7: OSPA errors regarding different quantile values at the final epoch in Test 1 (10 MCs)

		5%	25%	50%	75%	95%
PHD	Position (m)	221.642	396.127	568.393	873.224	1495.539
	Velocity (m/s)	0.026	0.038	0.049	0.080	0.134
Consider PHD	Position (m)	339.654	351.854	608.244	775.457	1432.741
	Velocity (m/s)	0.028	0.038	0.054	0.070	0.128

Test 1

First a simple scenario is tested. Angles and angular rate measurements are generated for two geostationary objects (Object 1 and Object 2) in 10 Monte Carlo simulations (MCs). They are assumed to be in the FOV of the telescope camera for one night. 15 measurements are randomly collected within a time duration of four hours. The detection probability is given as 1, which means no miss detections. No clutter measurements are considered. The OSPA

distances for position and velocity and the estimated cardinality using the PHD filter and consider PHD filter are given in Fig. 1 and Fig. 2, respectively. Different curve patterns indicate different quantile values. For both filters, the 95% quantile curves have the largest OSPA error.

It is indicated from two figures that both filters converge as OSPA errors for position and velocity reduce along with the time. The cardinality of each filter stays at two through the simulation time. The consider PHD filter achieves faster convergence than the PHD filter as shown in the OSPA curves at approximately the 5th epoch. Position and velocity OSPA errors regarding different quantile values for the last epoch are shown in Table 6. The consider PHD filter does not outperform the PHD filter for each of these metrics.

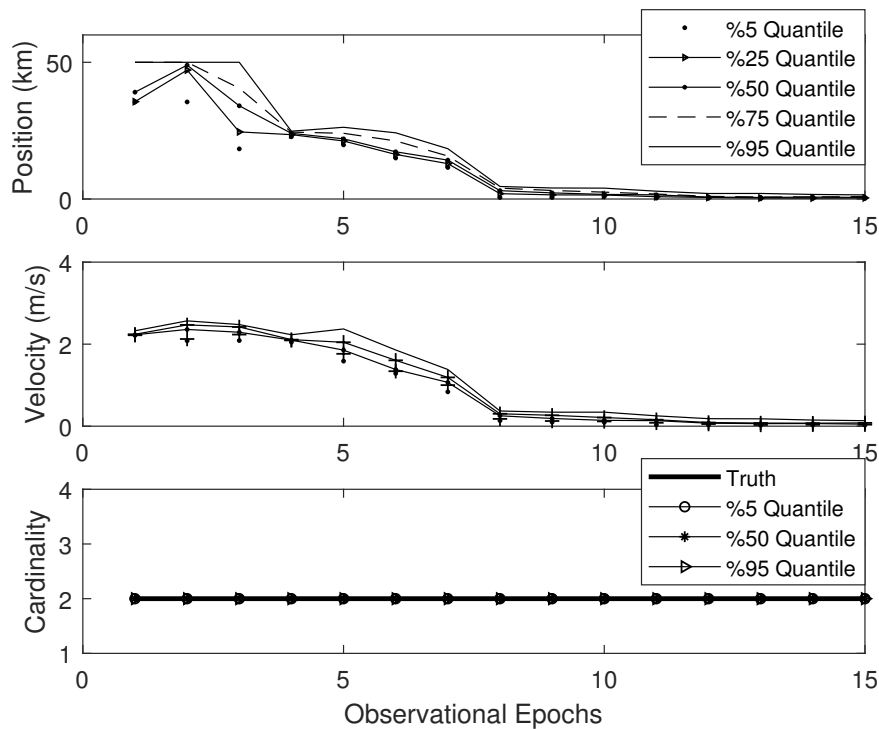


Fig. 1: OSPA distances and estimated cardinality using the PHD filter in Test 1 (10 MCs)

Test 2

In this test, 100 MCs are executed in a tracking window of two nights with a total of 30 measurements randomly generated. Both object birth and death are considered for a more realistic scenario. Object 3 is modelled as birth from the 5th epoch and its Keplerian elements are Object 2 dies at the 21th epoch. The detection probability is given as 0.99. The FOV of the camera is set as $[-1.2^\circ, 1.2^\circ]$ for right ascension and $[-2.4^\circ, 2.4^\circ]$ for declination. The Poisson average rate of the uniform clutter is given as 1 per scan. Fig. 3 and Fig. 4 depict the OSPA distances for position and velocity and the estimated cardinality using the PHD filter and the consider PHD filter, respectively. Different curve patterns indicate different quantile values.

Position and velocity OSPA errors regarding different quantile values for the last epoch are shown in Table 8. The consider PHD filter outperforms the PHD filter in terms of position OSPA errors regarding all quantile values except for the 25% quantile value. Regarding the velocity OSPA error of the last epoch, the consider PHD filter outperforms the PHD filter. Table 9 gives the statistical OSPA errors for two filters in 100 MCs. It is shown that the

consider PHD filter has slightly smaller errors than the PHD filter for both position and velocity in terms of mean, standard deviation and root mean square. The OSPA distances and estimated cardinality using two filters are given in Figs. 3 and 4. After one night, both filters tend to converge so the OSPA errors decrease. It is clearly both two filters suffer from the cardinality estimation biases for the first night but can track the survival space objects at the last stage. The consider PHD filter has less cardinality estimation error jumps than the PHD filter. That is why the consider PHD filter yields better accuracy in terms of statistical values shown in Table 9.

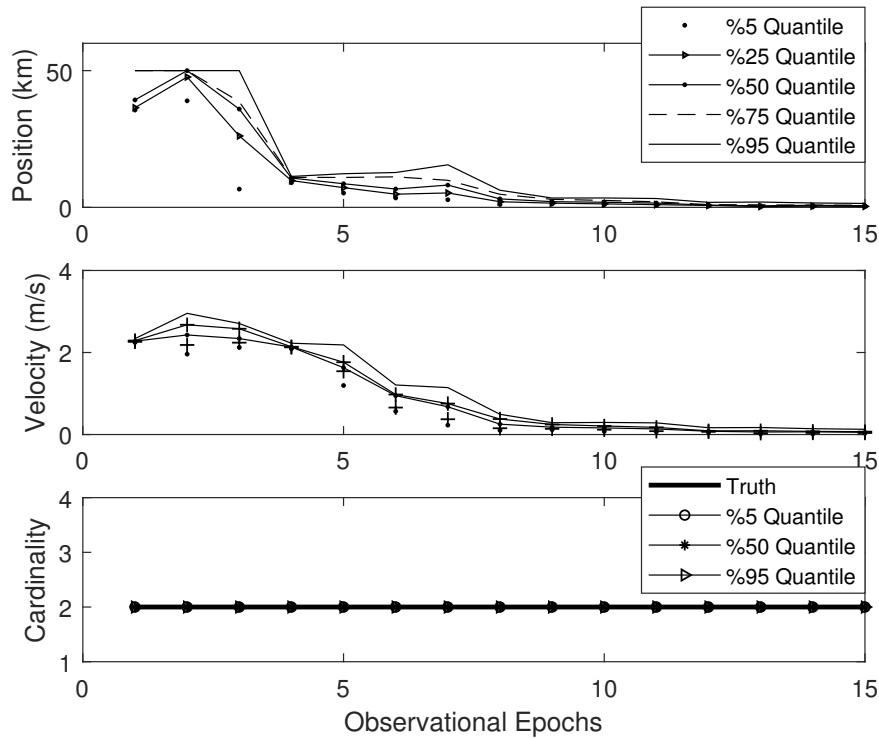


Fig. 2: Consider OSPA distances and estimated cardinality using the Consider PHD filter in Test 1 (10 MCs)

Table 8: OSPA errors regarding different quantile values at the final epoch in Test 2 (100 MCs)

		5%	25%	50%	75%	95%
PHD	Position (m)	478.311	797.425	1318.395	1766.658	3593.953
	Velocity (m/s)	0.053	0.087	0.138	0.193	0.387
Consider PHD	Position (m)	462.988	822.837	1275.849	1717.856	3522.868
	Velocity (m/s)	0.050	0.087	0.133	0.183	0.380

Table 9: Statistical OSPA errors for 100 MCs in Test 2

		Mean	Standard Deviation	Root Mean Square
PHD	Position (km)	14.563	13.313	19.581
	Velocity (m/s)	1.949	2.163	2.884
Consider PHD	Position (km)	14.555	13.294	19.563
	Velocity (m/s)	1.943	2.160	2.878

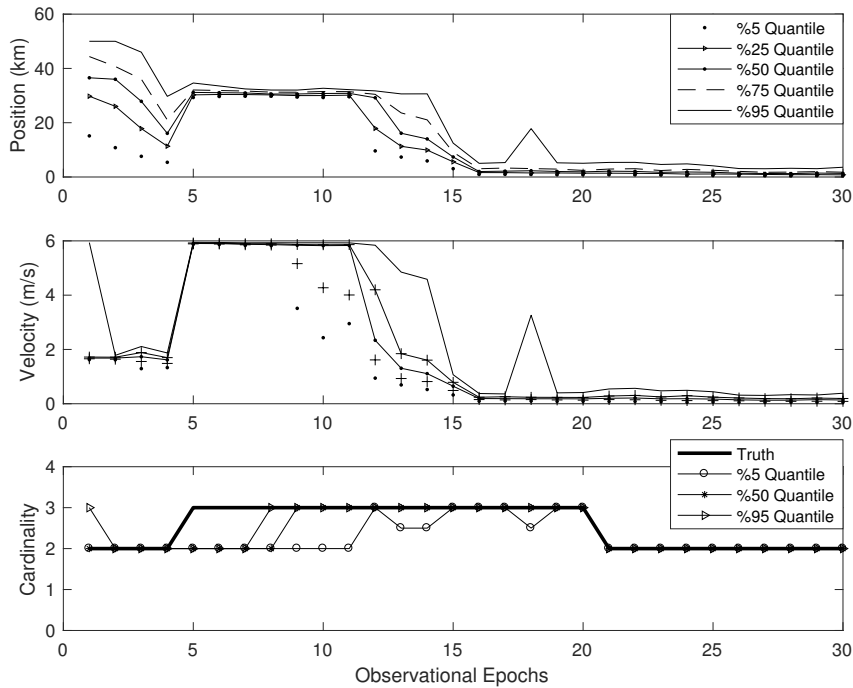


Fig. 3: OSPA distances and estimated cardinality using the PHD filter in Test 2 (100 MCs)

Test 3

Based on the settings in Test 2, this test further considers closely orbiting space objects. A lower detection probability of 0.95 is used for testing different filters. In Fig. 5, the left subfigure depicts the angular measurements, i.e., right ascension and declination, generated for three space objects, and the right subfigure depicts angle difference of Object 4 and 5 with respect to Object 1. Note that to generate these plots, no clutter measurements are considered, and the probability of detection is given very closely to 1. But the test scenario considers the clutter return and a detection probability of 0.95. Obviously, all three space objects can be captured by the FOV of the telescope camera.

100 MCs are executed. The OSPA errors regarding different quantile values at the final epoch are compared in Table 9 for two filters. The consider PHD filter only generates smaller position OSPA errors in terms of the 95% quantile value in compared to the PHD filter. OSPA distances and estimated cardinality using two filters are plotted in Fig. 7 and 8, respectively. It is shown that the 5% quantile cardinality estimation via two filters are both suffering one space object loss compared to the truth. There is much chance that the close distances among three space objects lead to the cardinality estimation biases, and these biases result in larger OSPA errors of 50%, 75% and 95% quantile than 5% quantile for two PHD filters. The 5% quantile OSPA position and velocity errors have spikes via the PHD filter while those error are more stable via the consider PHD filter at the final stage of the simulation. The statistical OSPA errors by the consider PHD filter are smaller than the PHD filter for the standard deviation and root mean square of both position and velocity results, which is shown in Table 10.

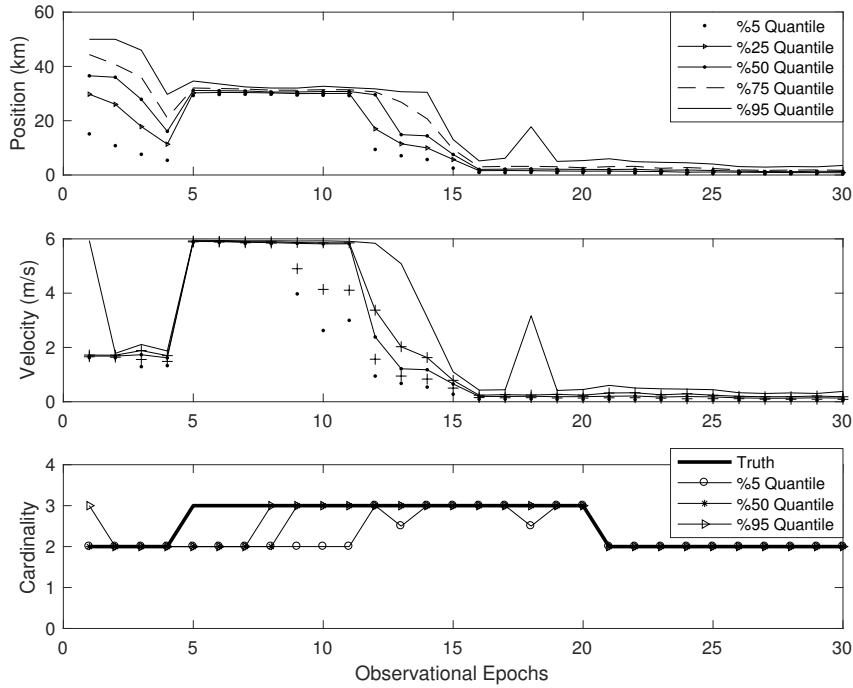


Fig. 4: OSPA distances and estimated cardinality using the Consider PHD filter in Test 2 (100 MCs)

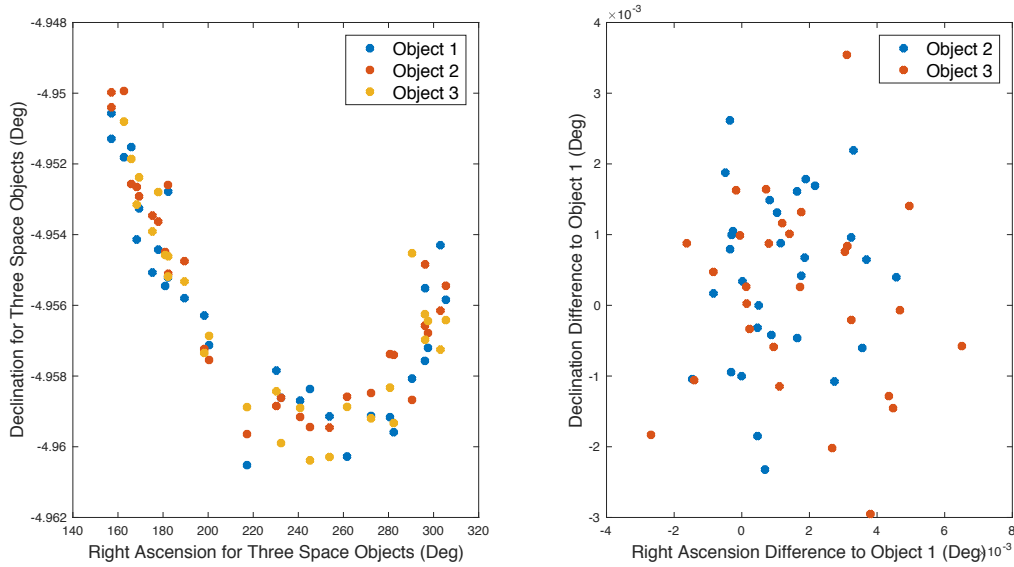


Fig. 5: Angular measurements and angle difference for all Object Tracks

Table 9: OSPA errors regarding different quantile values at the final epoch in Test 3 (100 MCs)

		5%	25%	50%	75%	95%
PHD	Position (m)	1208.757	2092.179	25016.874	25108.112	28968.434
	Velocity (m/s)	0.087	0.173	5.001	5.004	5.777
Consider PHD	Position (m)	1496.866	2977.776	25061.868	25123.446	28961.512
	Velocity (m/s)	0.130	0.274	5.002	5.005	5.777

Table 10: Statistical OSPA errors for 100 MCs in Test 3

		Mean	Standard Deviation	Root Mean Square
PHD	Position (km)	27.039	17.899	32.261
	Velocity (m/s)	4.920	3.561	6.039
Consider PHD	Position (km)	27.845	12.990	30.634
	Velocity (m/s)	4.994	2.858	5.731

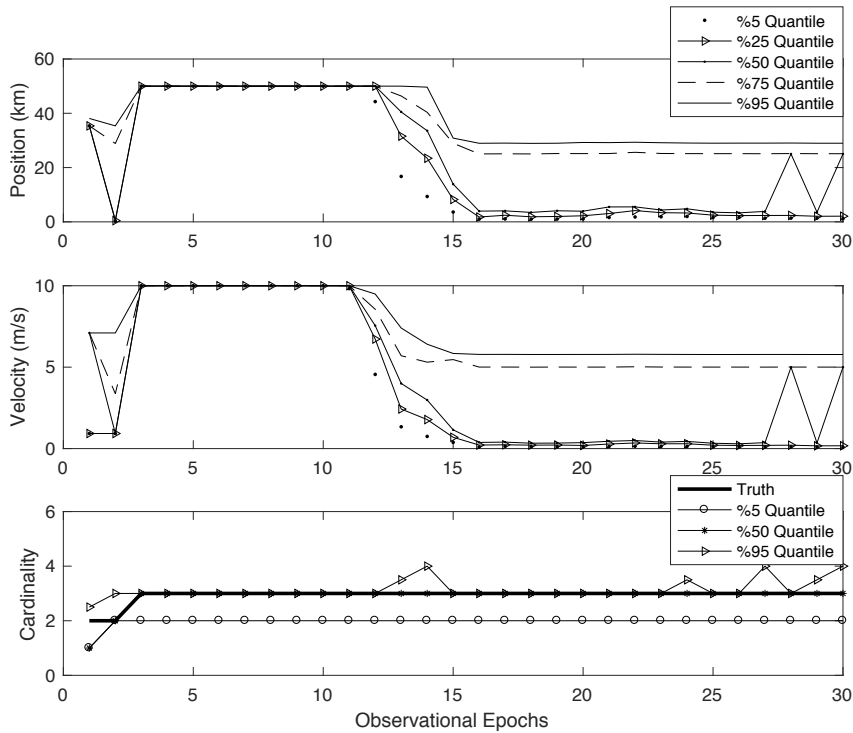


Fig. 7: OSPA distances and estimated cardinality using the PHD filter in Test 3 (100 MCs)

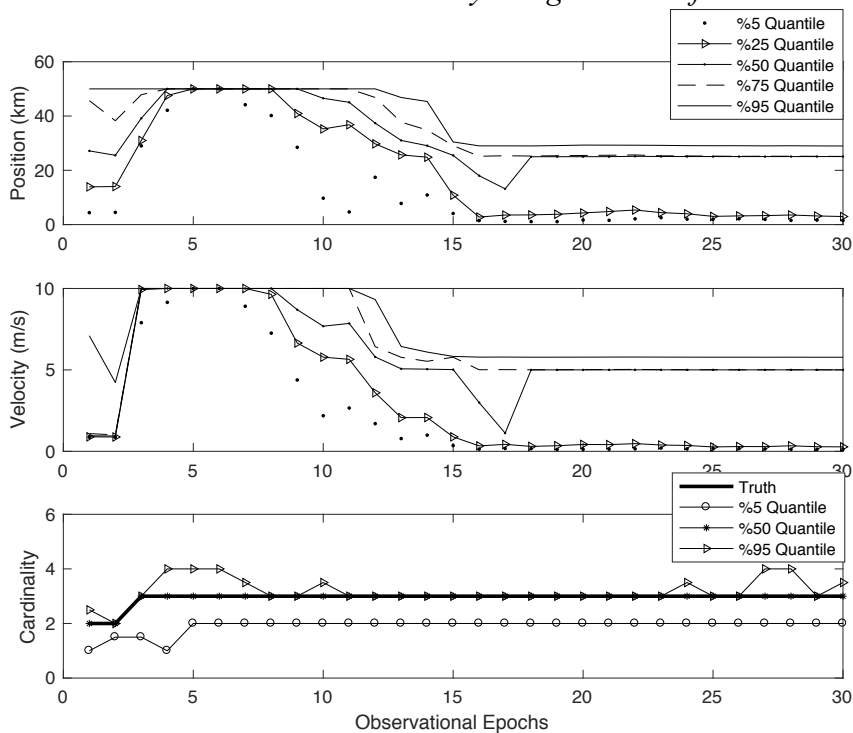


Fig. 8: OSPA distances and estimated cardinality using the Consider PHD filter in Test 3 (100 MCs)

Conclusions

This paper presents a consider probability hypothesis density filter for multi-object tracking as applied to the specific space tracking problem. With the help of the consider filter scheme, the uncertainty associated with the area-to-mass ratio can be taken into consideration. Hence, an improved multi-object tracking performance in terms of statistical OSPA errors is achieved by the consider PHD filter in comparison to the conventional PHD filter. However, it is known that the PHD filter follows the Poisson assumption for the object number (cardinality) distribution, which yields deteriorated performance in the object number estimates as shown in Test 3 as the “object death” phenomenon. This phenomenon becomes even more obvious with lower probability of detection and closely located space objects. Hence the OSPA errors surge to large values accordingly. Future work will be focused on integrating the consider scheme into more accurate multi-Bernoulli approximation filters, e.g., the labeled multi-Bernoulli filter, for the space object tracking problem.

Acknowledgement

The authors would like to acknowledge the support of the Cooperative Research Centre for Space Environment Management (SERC Limited) through the Australian Government’s Cooperative Research Centre Programme.

References

1. US National Aeronautics and Space Administration, “Space debris and human spacecraft,” https://www.nasa.gov/mission_pages/station/news/orbital_debris.html. Latest Accessed: 2018-12-10.
2. S. Blackman and R. Popoli, Design and analysis of modern tracking systems. Artech House, 1999, 10.1182/blood-2017-02-768176.
3. T. E. Fortmann, Y. Bar-Shalom, and M. Scheffe, “Multi-target tracking using joint probabilistic data association,” 1980 19th IEEE Conference on Decision and Control including the Symposium on Adaptive Processes, Dec 1980, pp. 807–812, 10.1109/CDC.1980.271915.
4. R. P. Mahler, Advances in statistical multisource-multitarget information fusion. Boston: Artech House, 2014.
5. B.-N. Vo and W.K. Ma, “The Gaussian mixture probability hypothesis density filter,” IEEE Transactions on Signal Processing, Vol. 54, Nov 2006, pp. 4091–4104, 10.1109/TSP.2006.881190.
6. B. Vo, B. Vo, and A. Cantoni, “Analytic implementations of the cardinalized probability hypothesis density filter,” IEEE Transactions on Signal Processing, Vol. 55, July 2007, pp. 3553–3567, 10.1109/TSP.2007.894241.
7. B. T. Vo and B. N. Vo, “Labeled random finite set sand multi-object conjugate priors,” IEEE Transactions on Signal Processing, Vol. 61, July 2013, pp. 3460–3475, 10.1109/TSP.2013.2259822.
8. J. S. McCabe and K. J. DeMars, “Considering uncertain parameters in non-Gaussian estimation for single-target and multitarget tracking,” Journal of Guidance, Control, and Dynamics, Vol. 40, Jul 2017, pp. 2138–2150, 10.2514/1.G002785.
9. K. Panta, D. E. Clark, and B. N. Vo, “Data association and track management for the gaussian Mixture probability hypothesis density filter,” IEEE Transactions on Aerospace and Electronic Systems, 2009, 10.1109/TAES.2009.5259179.
10. S. Gehly, Estimation of geosynchronous space objects using finite set statistics filtering methods. PhD thesis, 2016.
11. B. A. Jones, “CPHD filter birth modeling using the probabilistic admissible region,” IEEE Transactions on Aerospace and Electronic Systems, 2018, 10.1109/TAES.2018.2793378.

12. H. Cai, S. Gehly, Y. Yang, and K. Zhang, "Modeling birth for the labelled multi-Bernoulli filter using a boundary value approach," *Journal of Guidance, Control, and Dynamics*, Submitted in 2017.
13. S. Gehly, B. Jones, and P. Axelrad, "An AEGIS-CPHD filter to maintain custody of GEO space objects with limited tracking data," *Advanced Maui Optical and Space Surveillance Technologies Conference*, Sept. 2014.
14. Drew P. Woodbury and John L. Junkins. On the consider Kalman filter. In *AIAA Guidance, Navigation, and Control Conference*, AIAA Paper: 2010-7752. American Institute of Aeronautics and Astronautics (AIAA), August 2010.
15. Jason Stauch and Moriba Jah. Unscented Schmidt-Kalman filter algorithm. *Journal of Guidance, Control, and Dynamics*, 38(1):117-123, January 2014.
16. J. L. Geeraert and J. W. McMahan. Square-Root unscented Schmidt-Kalman filter. *Journal of Guidance, Control, and Dynamics*, 41(1): 278-285, January 2018.
17. D. Schuhmacher, B. T. Vo, and B. N. Vo, "A consistent metric for performance evaluation of multi-object filters," *IEEE Transactions on Signal Processing*, 2008, 10.1109/TSP.2008.920469.
18. B. A. Jones and B. N. Vo, "A labeled multi-Bernoulli filter for space object tracking," *Proc.AAS/AIAA Spaceflight Mech. Meeting*, 2014, pp. 11-15.
19. O. Montenbruck and E. Gill, *Satellite orbits: models, methods, and applications*. Springer, 2000.